Communications in Computational Chemistry
Commun. Comput. Chem. Vol. 8, No. 1, 44–53
doi: 10.4208/cicc.2025.252.01
Regular Article

Excited-State Decay Paths of Ortho-Terphenyl: Electronic Structure Calculations and Nonadiabatic Dynamics Simulations

Jia-Ling Dai[1], Rui Zhao[1] and Bin-Bin Xie[1,*]

[1] *Hangzhou Institute of Advanced Studies, Zhejiang Normal University, 1108 Gengwen Road, Hangzhou 311231, Zhejiang, P. R. China.*

[*] Corresponding author: binbinxie@zjnu.edu.cn.

Received 9 Sept. 2025; Accepted (in revised version) 13 Jan. 2026

Abstract: Photoexcitation of *ortho*-terphenyl (OTP) to cyclize into *4a,4b*-dihydrotripheneylene (DHT) is regarded as the first step in the synthesis of triphenylene. Surprisingly, the nonadiabatic cyclization mechanisms of this textbook reaction have not been examined explicitly until now. Herein we focus on the photoinduced dynamics of OTP by using static electronic structure calculations (MS-CASPT2//CASSCF) and trajectory-based surface-hopping dynamics simulations (OM2/MRCI). In terms of the calculated results, we shed light on two distinct relaxation pathways from the S_1 state and also the mechanism of photocyclization. The pyramidalization of central benzene ring and the subsequent $S_1 \rightarrow S_0$ transition via the S1S0-OTP intersection region is the predominant route (PATH I, ~ 81.5%); while the relaxation from the S_1 state to the S_0 state through the S1S0-DHT intersection region is the minor pathway and can be determined to be the key step for the formation of DHT conformer in the ground state (PATH II, ~ 11.3%). In the simulated period of 3.0 ps, the final recovery yield of S_0 OTP conformer is predicted to be 92.8% due to thermally activated ring reopening of DHT conformer; that is, the intermediate DHT is not so stable in the ground state. In addition, two relaxation time constants (538.7 fs and 5.1 ps) are predicted for the S_1 dynamics of OTP with the faster process assigned to the nonreactive deactivation (PATH I) and the slower one assigned to the ring closure reaction (PATH II), which are well consistent with the experimental values of 700 fs and 3.0 ps in the solutions of tetrahydrofuran (THF). Finally, the present work can provide important photocyclization mechanistic insights for OTP system and also the similar *ortho*-arenes.

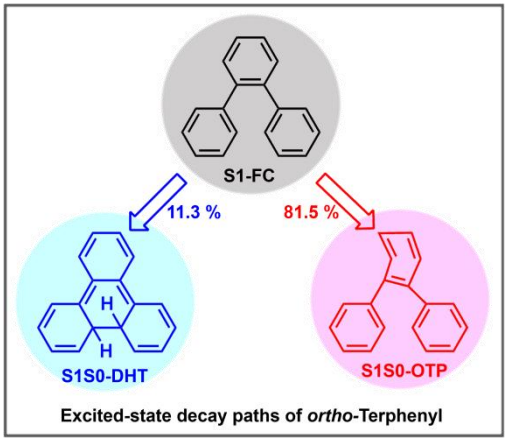

Key words: ortho-terphenyl, excited-state decay, nonadiabatic dynamics, photo-cyclization.

1. Introduction

Nonadiabatic transitions between different electronic states are very important in the photo-induced chemical, biological, and material systems, involving deactivation of excited states, photo-dissociation of small molecules, photo-isomerization of large biological systems, and nonadiabatic recombination of charge carriers of photovoltaic materials, and so on [1-9]. Since the first observation of photo-induced carbon-carbon bond formation in stilbenes and related systems in the first mid-20th century, much attention has been attracted to investigate the photochemical cyclization behaviors [10-15]. Photocyclization reactions have been applied to various fields, such as light-assisted synthesis of ployaromatic compounds and design of molecular photo-switches [14-25]. For instance, photocyclization reaction has been used to synthesize pharmaceuticals (e.g., antibiotics and antitumor agents) [23-25] and large polycyclic aromatic hydrocarbon materials (e.g., graphite ribbons) [20,21]. Besides, photocyclization has also been utilized to design molecular photo-switches for the applications in memory storage and chemical sensitization [19,22].

In addition to the above fundamental applications, experimental and computational scientists have also been dedicated to studying the underlying mechanisms of photocyclization reactions, especially, for identifying the relationships of molecular structures – potential energy surfaces – nonadiabatic chemical dynamics [26-38]. In the present work, we will concentrate on the nonadiabatic photocyclization reaction of an ideal system *ortho*-

terphenyl (OTP), which can structurally prohibit the cis-trans isomerization reaction and help to clarify the detail mechanisms of the ring-closure process. The photocyclization of OTP system into the intermediate 4a,4b-dihydrotriphenylene (DHT) is regarded as the first step to synthesize triphenylene [14-16] (see this textbook reaction in Scheme 1). Previously, Bragg's group has made lots of effort to elucidate the structure – dynamics relationships of a series of *ortho*-arenes and related systems [26-30]. In 2013, Smith et al [30]. explored the ultrafast excited-state dynamics of OTP and 1,2-diphenylcyclohexene (DPCH) in THF solution. Ultrafast time-resolved spectral dynamics reflected that both systems could undergo cyclization on picosecond time scales with the S_1-to-S_0 transition faster for DPCH versus OTP; in combination with the *ab initio* calculations, they also suggested that OTP system needs to overcome a larger energy barrier than DPCH system to approach the intersection region and this motion is of high relevance to "ethylenic" twisting dihedral angle. One year later, Molly and coworkers [29] studied the solvent effects on the photocyclization of OTP system. Femtosecond transition absorption spectroscopy demonstrated that a solvent-dependent nonadiabatic cyclization with a time scale of 1.5 – 4.0 ps. They also found that the solvent-solute mechanical interactions have a significant influence on the nonadiabatic processes and facilitate vibrational relaxation of DHT in the period of 10-25 ps. In addition, DHT system will undergo thermally activated ring-opening reaction with a lifetime of ~ 46 ns in THF. In recent works, they investigated the photocyclization in structurally modified *ortho*-terphenyls, ranging from phyenyl-substituted OTP (i.e., 1,2,3-triphenylbenzene (TPB) and ortho-quaterphenyl (OQTP)) to methyl-, *tert*-butyl-, *tert*-butyl-, and trifluoromethyl-substituted OTP [27,28]. In terms of the results from time-resolved spectroscopy and theoretical calculations, they demonstrated how structural modifications change the excited-state dynamics and photocyclization mechanisms. More recently, by using pump-repump-probe (PRP) transient hole burning technique, they revisited the photocyclization reaction of OTP system, especially, for the excited-state reaction pathways [26]. Transient absorption spectroscopy studies revealed two decay time scales (700 fs and 3.0 ps), but neither could unambiguously be assigned to DHT formation. The PRP method could clarify these two processes with the fast one belonging to the nonreactive deactivation and the slow one to the photocyclization of S_1 OTP. However, they couldn't provide more detailed mechanisms, including the branching ratios of excited state relaxation channels and also the structure of the nonreactive deactivation.

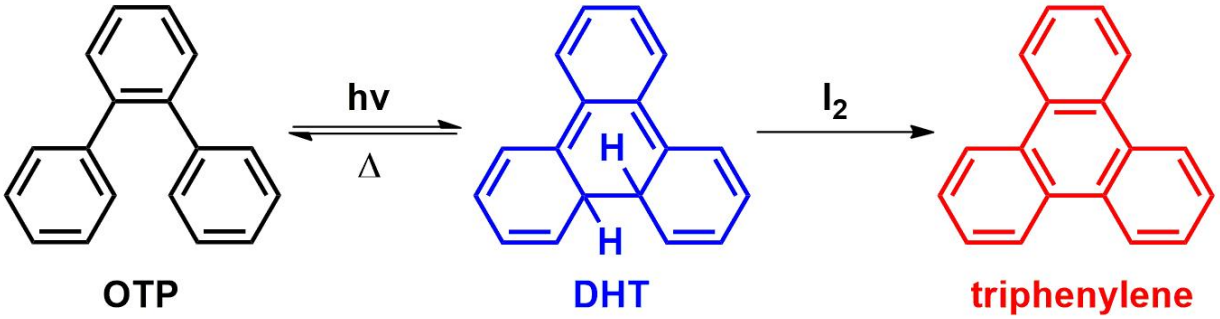

Scheme 1. Photo-induced cyclization and dehydrogenation of *ortho*-terphenyl.

Herein, the high-level static electronic structure calculations (MS-CASPT2//CASSCF and OM2/MRCI methods) and trajectory-based surface-hopping nonadiabatic dynamics simulations (OM2/MRCI approach) will be carried out to clarify the following unsolved questions: (i). the branching ratios of different excited-state relaxation channels; (ii). the intersection structures of reactive and nonreactive deactivation pathways; (iii). the thermally activated ring-opening between the OTP and DHT in the ground state. Our current work will present a systematically study on photocyclization of the OTP system and will also contribute to providing important mechanistic insights on similar *ortho*-arenes.

2. Computational details

***Ab initio* calculations.** The S_0 conformers and vertical excitation energies of *ortho*-terphenyl (OTP) and *4a,4b*-dihydrotriphenylene (DHT) were first obtained by using the DFT and TD-DFT methods with the B3LYP and CAM-B3LYP functionals, respectively [39-45]. Then, the calculations of minima, conical intersections, linearly interpolated internal coordinate paths (LIIC), and minimum-energy paths (MEP) were performed at two-state-averaged complete active space self-consistent field (SA2-CASSCF) level with equal state weights for the S_1 and S_0 states. The active space comprised 12 π electrons in 10 π* orbitals, referred to as SA2-CASSCF(12,10) hereinafter (see **Figure S1**). Dynamic correlation effects were taken into account with the multi-state complete active space second-order perturbation approach (MS-CASPT2) [46,47] to re-evaluate the energies of all optimized structures, LIIC, and MEP paths. In the MS-CASPT2 energy evaluations, the standard zeroth-order Hamiltonian (IPEA=0.25) was used [48]; the imaginary level shift of 0.2 au was used to minimize the presence of intruder states [49]; the Cholesky decomposition technique with unbiased auxiliary basis sets was used for accurate two-electron integral approximations [50]. The 6-31G* basis set was applied for all structural optimizations and single-point energy calculations [51,52]. The above *ab initio* calculations were carried out using the following programs: GAUSSIAN09 for DFT and TD-DFT calculations [53]; OpenMolcas for SA2-CASSCF optimizations and MS-CASPT2 computations [54,55].

Semiempirical methods. Geometry optimizations and dynamics simulations were calculated at OM2/MRCI level with analytical evaluations of the energies, gradients, and nonadiabatic coupling terms. The Lagrange–Newton approach was employed to optimize the minimum-energy conical intersections [56,57]. The restricted open-shell Hartree-Fock formalism was applied to the SCF treatment in our OM2/MRCI calculations, which was demonstrated to be able to give an accurate description of structures and energies in the ground and excited states. The active space comprised 14 electrons in 14 orbitals, that is, the six highest doubly occupied orbitals, two singly occupied orbitals, and six

lowest unoccupied orbitals. The MRCI treatment included three reference configurations that can be generated from the HOMO and LUMO of the closed-shell ground state. Thus, the MRCI wavefunction was built by allowing all single and double excitations from these three references.

Nonadiabatic dynamics simulations. Photoinduced S_1 nonadiabatic dynamics was carried out using trajectory-based surface-hopping simulations (OM2/MRCI method) with the initial atomic coordinates and velocities randomly sampled from a S_0-state trajectory (10 ps, 300 K, *NVT* ensemble). Then, the computed S_0–S_1 transition probabilities were used to further screen the excited-state dynamic runs, specifically, the configurations with very small transition probabilities were excluded. For the present nonadiabatic dynamics simulations, the nuclear degrees of freedom were propagated on 3.0 ps classical trajectories with a time step of 0.1 fs (the velocity-Verlet algorithm), while the evolution of the quantum degrees of freedom along these trajectories was evaluated by using a unitary propagator with a time step chosen to be 200 times smaller (0.0005 fs). The fewest switching algorithm was applied to compute the hopping probabilities for the point with an energy gap less than 10 kcal/mol. All simulations were performed in the adiabatic representation with all relevant energies, gradients, and nonadiabatic coupling vectors being computed on-the-fly as needed. The empirical decoherence correction scheme (0.1 au) proposed by Granucci et al. was employed [58] and the translational and rotational motions were removed in each step. The final results were obtained by averaging over 390 trajectories that finished successfully in the S_1 photo-dynamics. All the above semiempirical electronic structure calculations and dynamics simulations were performed using the OM2/MRCI method as implemented in the MNDO99 program [59-61]. For more computational details, please refer to our previous publications [13,17,18,62-65].

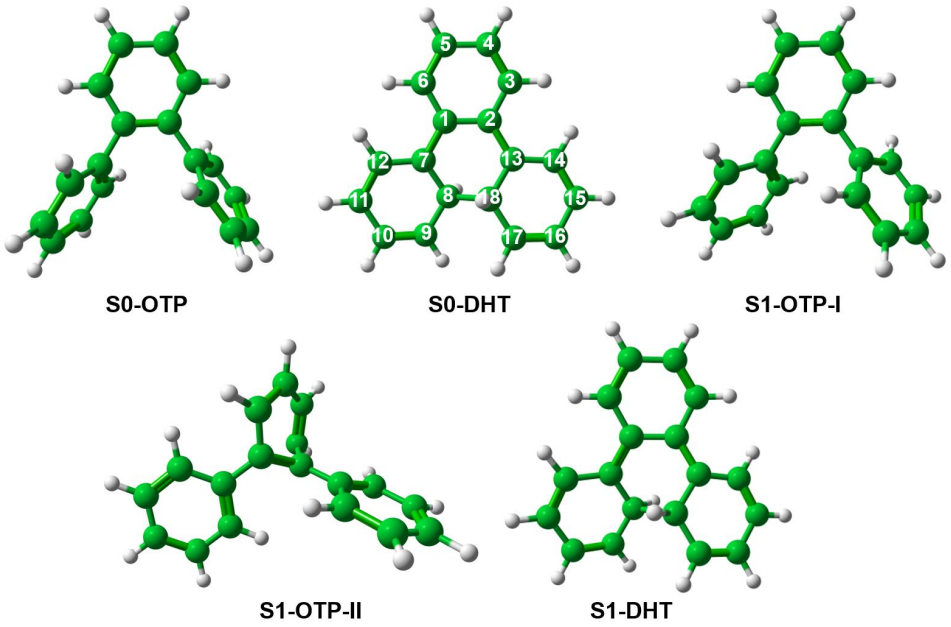

Figure 1. The optimized S_0 and S_1 minima of OTP and DHT systems at the SA2-CASSCF level. See **Table S1** for key geometric parameters at both SA2-CASSCF and OM2/MRCI levels.

3. Results and discussion

3.1 Electronic structure calculations of *ortho*-terphenyl

Spectroscopic properties. First of all, we have obtained two stable ground-state conformers, i.e., S0-OTP and S0-DHT, by using the B3LYP, CAM-B3LYP, OM2/MRCI, and SA2-CASSCF methods. As is shown in **Figure 1** and **Table S1**, all these calculations predict similar stable structures in C_2 symmetry for both S0-OTP and S0-DHT conformers. The relative energies in **Table 1** clearly show that the most stable S_0 conformer is S0-OTP, which is computed to be 62.3 [63.9] kcal/mol lower than that of S0-DHT at the MS-CASPT2 [OM2/MRCI] level. Thus, the S0-OTP conformer would be predominant in the ground state, according to the Maxwell-Boltzemann distribution. The computed vertical excitation energies for the low-lying S_1 state of S0-OTP are listed in **Table 2** along with the related experimental values. The S_0-S_1 vertical excitation energy is overestimated by TD-CAM-B3LYP, OM2/MRCI, and MS-CASPT2 computations, which is ~ 0.3 [~ 0.5] eV higher than the maximum UV absorption in alcohol [the pump pulses in THF solvent]. Götze et al. noted that the vertical excitation energies are often higher than experimental peaks because experiments capture vibrationally relaxed states. And this is mainly caused by the combined effect of reorganization energy and ground state destabilization [66]. Electronic configurations analysis indicates that the lowest excited singlet state $S_1(\pi\pi^*)$ is a spectroscopically bright state with the relevant molecular orbitals localized on the central benzene ring as shown in **Figure 2**. Moreover, the S_1 state of OTP system is a mixed state and can be mainly derived by a single excitation from HOMO-1 to LUMO (weight: 0.302) and from HOMO to LUMO+1 (0.386). Overall, the OM2/MRCI and MS-CASPT2//CASSCF methods represent reasonable choices for computing of excited-state properties of OTP the S_1 state.

Table 1. MS-CASPT2//CASSCF [OM2/MRCI] computed adiabatic excitation energies (kcal/mol) of minima and intersection structures of OTP and DHT systems.

S0-OTP	0.0 [0.0]	S1-DHT	91.8 [97.8]
S0-DHT	62.3 [63.9]	S1S0-OTP	107.4 [110.9]
S1-OTP-I	104.2 [97.0]	S1S0-DHT	104.3 [109.8]
S1-OTP-II	107.7 [108.7]		

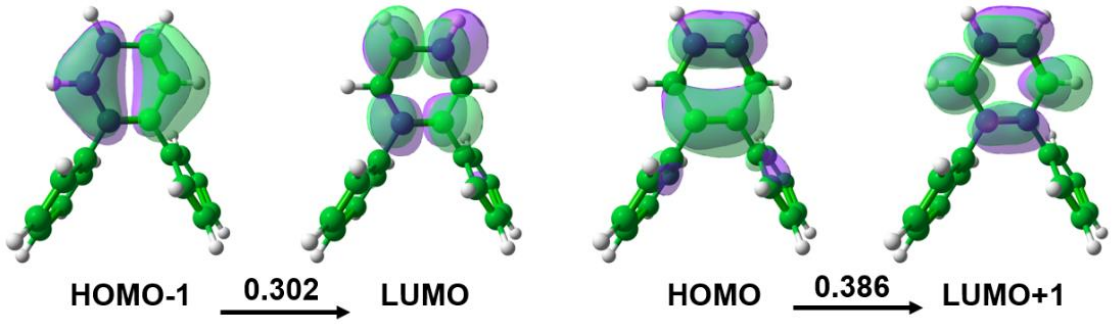

Figure 2. Primary molecular orbitals related to $S_0 \rightarrow S_1$ electronic transition of the S0-OTP minimum at MS-CASPT2 level.

S_0 and S_1 geometric structures. The optimized molecular structures and relative energies of OTP and DHT conformers are collected in **Figure 1** and **Table 1**. As mentioned above, two types of minima in C_2 symmetry, i.e., S0-OTP and S0-DHT, have been found in the ground state at both SA2-CASSCF and OM2/MRCI levels. The b(C_1-C_7) and b(C_2-C_{13}) bond lengths, α(C_7-C_1-C_2) and α (C_1-C_2-C_{13}) angles, and ϕ (C_8-C_7-C_1-C_2) and ϕ (C_1-C_2-C_{13}-C_{18}) dihedral angles of S0-OTP are calculated to be 1.501 [1.485] Å, 68.8 [55.7]°, and 122.8 [121.7]° at the SA2-CASSCF [OM2/MRCI] level. However, in comparison with S0-OTP, the conjugate pattern of S0-DHT is changed according to its Lewis structure. For instance, the b (C_1-C_7) and b (C_2-C_{13}) [b (C_7-C_8) and b (C_{13}-C_{18})] bond lengths decrease [increase] dramatically; the ϕ(C_8-C_7-C_1-C_2) and ϕ(C_1-C_2-C_{13}-C_{18}) dihedral angles vary from 68.8 [55.7] to -4.0 [-11.2]° at SA2-CASSCF [OM2/MRCI] level. In addition, we have also optimized three equilibrium structures in the S_1 state, that is, S1-OTP-I, S1-DHT, and S1-OTP-II, respectively. The former two structures closely resemble those in the S_0 state. By contrast, the latter exhibits a pronounced twist with pyramidalization at the C_1 and C_2 atoms of the central benzene ring, a feature that primarily arises from sudden polarization effects [67]. The adiabatic excitation energies of S1-OTP-I, S1-OTP-II, and S1-DHT are predicted to be 104.2 [97.0], 107.2 [108.7], and 91.8 [97.8] kcal/mol, respectively, as listed in **Table 1**.

Table 2. MS-CASPT2//CASSCF [OM2/MRCI] computed vertical excitation energies (eV) of the S_0 minimum of OTP system.

	CAM-B3LYP	OM2/MRCI	MS-CASPT2	EXP.	
S_1	5.19	5.20	5.24	4.95[a]	4.66[b]

[a] *The maximum absorption in alcohol (250.5 nm); Handbook of chemistry and physics. 60th ed. Boca Raton, Florida: CRC press Inc., 1979, p. C-510;*

[b] *The UV pump pulses with a center wavelength of 266 nm in THF solvent.*

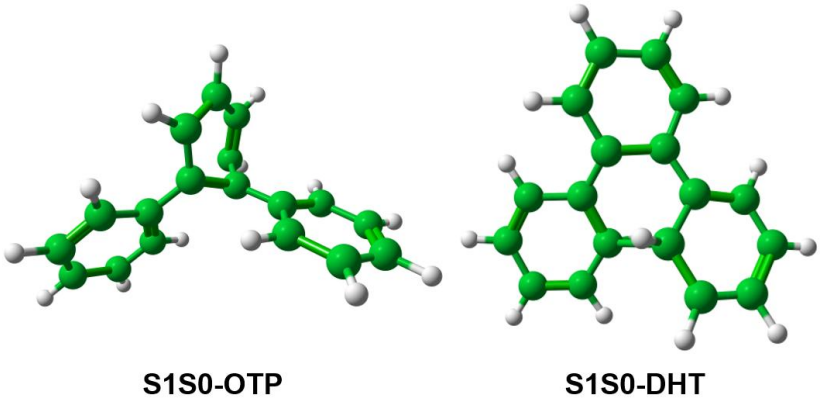

Figure 3. The optimized S_1/S_0 conical intersections of OTP and DHT systems at the SA2-CASSCF level. See **Table S1** for key geometric parameters at both SA2-CASSCF and OM2/MRCI levels.

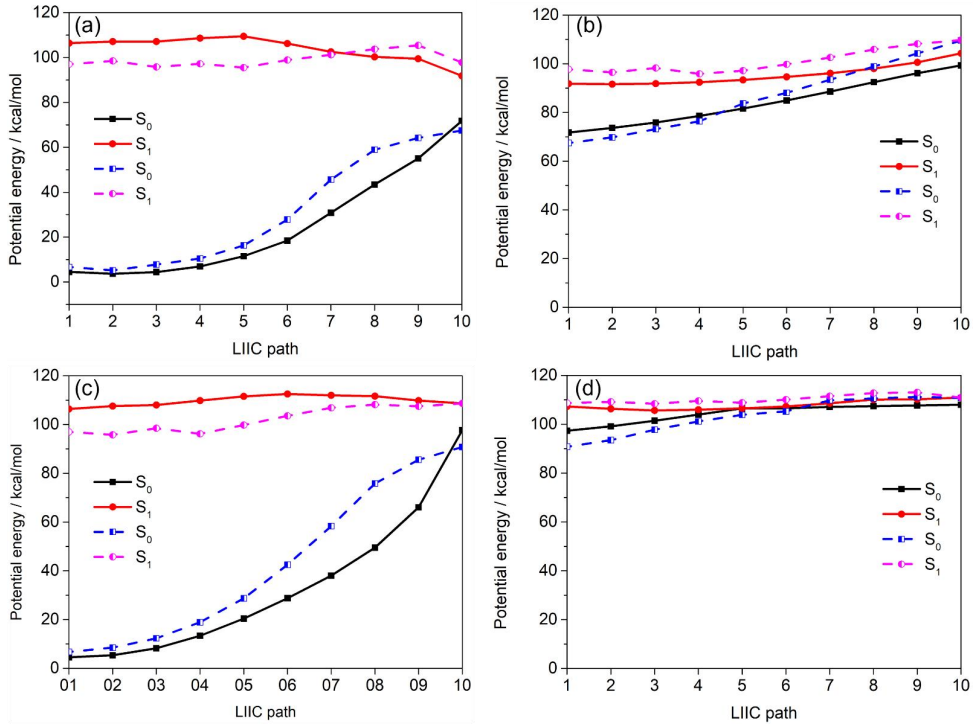

Figure 4. Linearly interpolated internal coordinate (LIIC) paths computed at MS-CASPT2 (solid line) and OM2/MRCI (dashed line) levels connecting S1-OTP-I and S1-DHT (a); S1-DHT and S1S0-DHT (b); S1-OTP-I and S1-OTP-II (c); and S1-OTP-II and S1S0-OTP (d).

S_1/S_0 conical intersections and excited-state decay paths. Two S_1/S_0 intersection structures, labeled as S1S0-OTP and S1S0-DHT in **Figure 3**, have been obtained by using SA2-CASSCF and OM2/MRCI methods. The structural overlaps in **Figure S2** shows that these two conical intersections are close to their corresponding S_1 minima, respectively, for example, S1S0-OTP [S1S0-DHT] is similar to S1-OTP-II [S1-DHT]. Besides, the adiabatic excitation energy of S1S0-DHT is about ~ 3.0 [~ 1.0] kcal/mol lower than that of S1S0-OTP at the MS-CASPT2 [OM2/MRCI] level. When only considering their potential energies, both S1S0-DHT and S1S0-OTP can be easily accessible from the S_1 Franck-Condon point (MS-CASPT2 [OM2/MRCI]: 120.8 [119.9] kcal/mol). Thus, these two intersection structures may play important roles in the S_1 decay processes.

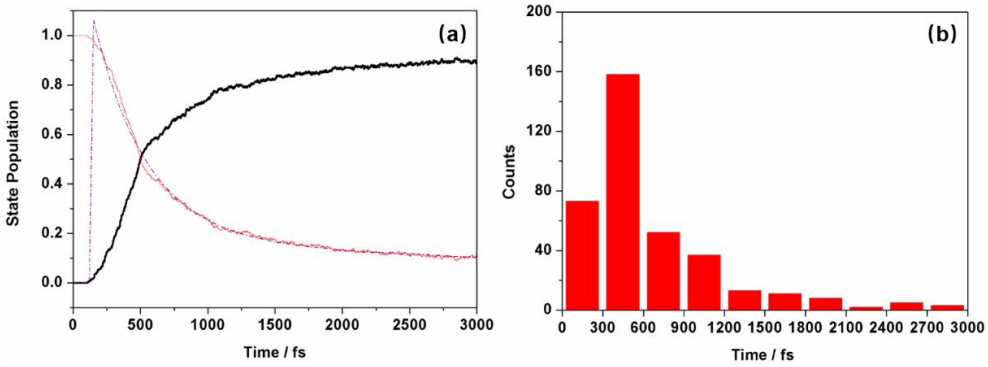

Figure 5. Time-dependent S_1 and S_0 state populations (a) and the distribution of $S_1 \rightarrow S_0$ hopping (b) in nonadiabatic dynamics simulations.

In addition, we have also explored the LIIC paths connecting the S_1 minima to the relevant S_1/S_0 intersection structures, that is, from S1-OTP-I to S1S0-DHT via S1-DHT (PATH II, **Figure 4a** and **Figure 4b**) and from S1-OTP-I to S1S0-OTP via S1-OTP-II (PATH I, **Figure 4c** and **Figure 4d**), respectively. As is shown in **Figure 4a**, it is apparent that there exists a ~ 1.5 kcal/mol barrier from the ring-opening conformer S1-OTP-I to the ring-closure conformer S1-DHT at the MS-CASPT2 level. Once arriving at the S_1 minimum S1-DHT, the system still needs to overcome a barrier of ~ 6.0 kcal/mol to get close to intersection region (point 8 to 9 of **Figure 4b**), where the energy gap between S_1 and S_0 states is less than 5.0 kcal/mol. Similarly, the S1-OTP-I minimum needs to overcome a very small energy barrier (~ 1.8 kcal/mol) to approach the S1-OTP-II minimum at the MS-CASPT2 level (**Figure 4c**). However, the S_1 potential energy curve connecting S_1-OTP-II and S_1S_0-OTP is rather flat, with the energy gaps between the S_1 and S_0 states remaining below 5.0 kcal/mol along the entire S_1 LIIC path (**Figure 4d**). In other words, the excited-state decay from the S_1 state to S_0 state could take place efficiently on this very wide and flat potential energy curve. It is important to note that the OM2/MRCI calculations yield a LIIC PESs that overall follows the same trend as those of MS-CASPT2, as illustrated in **Figure 4**. In order to consider the dynamic effects in the excited-state decay processes, the nonadiabatic dynamics simulations have been carried out in the next section.

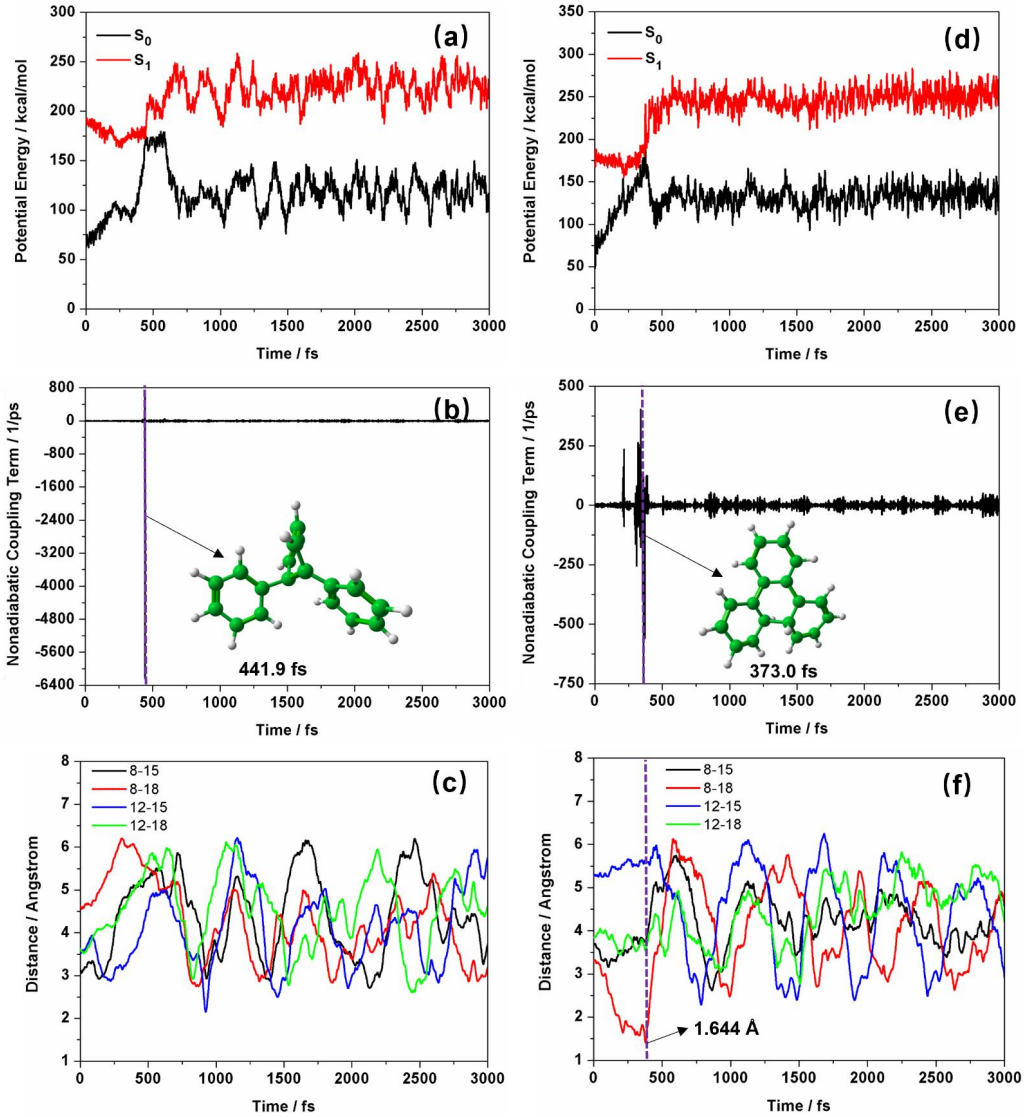

Figure 6. Potential energies, nonadiabatic coupling terms, and key bond lengths plotted as a function of time for the representative trajectories of type I (a, b and c) and type II (d, e and f). The hopping time is highlighted in vertical purple dash line along with the corresponding hopping structures.

3.2 Nonadiabatic dynamics simulations

Nonadiabatic dynamics. As discussed above, by comparison with the results with the MS-CASPT2//SA2-CASSCF approach, the semiempirical OM2/MRCI method can give reliably accurate excited-state potential energies, electronic and geometric structures. Moreover, the OM2/MRCI method can provide an accurate description to the S_0/S_1 intersection structures for both OTP and DHT systems, which can be easily seen from the structural overlaps between S1S0-OTP and S1S0-DHT conformers at both SA2-CASSCF and OM2/MRCI level in **Figure S3**. As a result, the OM2/MRCI-based surface-hopping nonadiabatic dynamics simulation has been carried out to study the S_1 photo-dynamics of OTP system to explore the excited-state decay pathways, lifetimes, and structural evolutions.

Among 390 successful trajectories in our dynamics simulations, 92.8% (362) trajectories decay to the S_0 state and 7.2% (28) still survive in the S_1 state at the end of 3.0 ps. The time-dependent S_1 and S_0 state populations along with the dot-dashed fitted line of the S_1 state are plotted in **Figure 5a**. A di-exponential equation $y = A_1^*\exp(-(x-x_0)/\tau_1) + A_2^*\exp(-(x-x_0)/\tau_2)$ is used to fit the time evolution of the S_1 population. The S_1 population keeps constant in the period of 148.0 fs (i.e., latency time x_0), which can be assigned to the initial relaxation from the S_1 Franck–Condon point to the S_1/S_0 intersection regions. We can estimate the S_1 state lifetimes τ_1 and τ_2 to be 390.7 and 4956.3 fs, with corresponding standard errors of 1.54% and 3.75%, respectively. Meanwhile, the corresponding weights A_1 and A_2 are fitted to be 0.85 and 0.15, respectively, which are close to the branching ratios of S1S0-OTP and S1S0-DHT to be 0.88 (318/362) and 0.12 (44/362) in our nonadiabatic dynamics simulations. Experimentally, by using transient absorption spectroscopy (TAS) and pump−repump−probe (PRP) spectroscopic tools, Snyder and Bragg revealed two relaxation time scales of OTP* (700 fs and 3.0 ps) and also determined that S_1 OTP only cyclizes on the slower of these time scales, with the faster process assigned to nonreactive deactivation [26]. However, they couldn't provide the branching ratios of excited-state relaxation channels and also the structure of the nonreactive deactivation.

The distribution of $S_1 \rightarrow S_0$ hopping-time in all nonadiabatic trajectories are plotted in panel b of **Figure 5b**. It clearly shows that about 80 percent of trajectories hop to the ground state within

1.0 ps, which numerically approaches the faster component of S_1 excited-state lifetime (700 fs) in TAS. Besides, there are still a few nonadiabatic trajectories that decay to the S_0 state after 2.0 ps, which coincides with the slower relaxation time scale of 3.0 ps in TAS.

Typical trajectories. Next we will move on to the typical trajectories in the present study. On the basis of the static electronic structure calculations, the S0-OTP conformer would be predominant in the ground state. Thus, upon irradiation at 266 nm, the system would be populated at the S_1 Franck-Condon region around the OTP conformer. All the successful OM2/MRCI-simulated nonadiabatic trajectories can be classified into two categories: (type I) Most of the nonadiabatic trajectories (318) are initially propagated into the S_1-OTP-II region via S_1-OTP-I. They subsequently decay to the ground state near the S_1S_0-OTP conical intersection, which can be assigned to the nonreactive channels; (type II) The remaining 44 trajectories relax directly to S_1-DHT, followed by an $S_1 \rightarrow S_0$ transition in the vicinity of the S_1S_0-DHT conical intersection, ultimately yielding the ring-closure conformer S_0-DHT. Time evolution of potential energies, nonadiabatic coupling terms, and also key bond lengths for two representative trajectories are plotted in **Figure 6**, respectively.

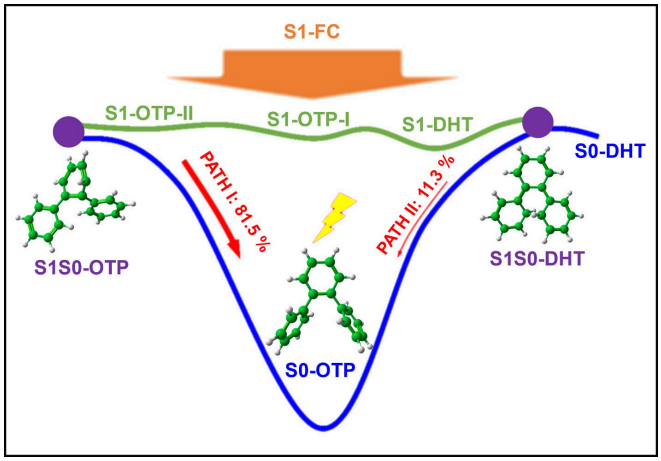

Figure 7. A proposed mechanistic diagram illustrating the excited-state decay pathways of OTP.

Upon irradiation at 266 nm, the representative trajectory of type I in **Figure 6a** and **Figure 6c** is initially populated in the S_1 Franck-Condon region. Then, the trajectory will be propagated into the S1-OTP-II region via S1-OTP-I minimum, where the central benzene ring is seriously twisted. As the S1S0-OTP conical intersection lies close to S1-OTP-II minimum (see **Figure S2**), the nonadiabatic trajectory will decay to the ground state soon at about 441.9 fs with a small energy gap (less than 2.0 kcal/mol) and a large nonadiabatic coupling term (ca. 6400 1/ps). In the representative trajectory of type II (see **Figure 6d** and **Figure 6f**), the system is first excited to the S_1 Franck-Condon region and then proceeds into an excited-state transient intermediate S1-DHT via the minimum structure S1-OTP-I. During this process, the C_8-C_{18} distance continuously decreases from 3.300 Å to 1.644 Å with a simple rotation of two terminal phenyl groups simultaneously. Later, this nonadiabatic trajectory is propagated into the S1S0-DHT region, where the potential energies of S_1 and S_0 states become degenerate and the nonadiabatic coupling term is predicted to be 750 1/ps. As a result, the system decays to the ground state directly at about 373.0 fs. Once the trajectory evolves in the ground state, the S0-OTP conformer will be regenerated due to thermally activated ring reopening of S0-DHT conformer, which is in line with the minimum-energy path between S0-OTP and S0-DHT in the S_0 state in **Figure S4**. Finally, it should be stressed that in our dynamic simulations, only a few trajectories decay to the S_0 state via the S1S0-DHT and most of the nonadiabatic trajectories relax to the ground state through the nonreactive deactivation pathway (S1S0-OTP).

4. Conclusion

In the present work, the high-level static electronic structure computations and nonadiabatic dynamics simulations (MS-CASPT2//CASSCF and OM2/MRCI approaches) are carried out to simulate photodynamics of the OTP system. These two methods can give reliably accurate potential energies, electronic and geometric structures (see the potential energies in **Table 1** and structural overlaps in **Figure S3**). On the basis of the optimized minima, intersection structures, LIIC, and MEP paths in S_0 and S_1 states, we have proposed two nonadiabatic relaxation pathways from the S_1 state to the S_0 state with high-efficiency.

Later, our proposed S_1 decay mechanism is immediately verified by the OM2/MRCI-based surface-hopping dynamics simulations. Two types of nonadiabatic processes are determined by the current dynamical simulations, which can be summarized as: S0-OTP + $h\upsilon \rightarrow S_1$(FC) $\rightarrow$ S1-OTP-I $\rightarrow$ S1-OTP-II $\rightarrow$ S1S0-OTP $\rightarrow$ S0-OTP (PATH I); S0-OTP + $h\upsilon \rightarrow S_1$(FC) $\rightarrow$ S1-OTP-I $\rightarrow$ S1-DHT $\rightarrow$ S1S0-DHT $\rightarrow$ S0-DHT $\rightarrow$ S0-OTP (PATH II). The nonreactive deactivation pathway via the S1S0-OTP (PATH I, 81.5%) is the predominant route with the C_1 and C_2 atoms of central benzene ring strongly twisted due to the sudden polarization effects (**Figure 7**). The other pathway (PATH II, 11.3%) is the minor one and the relaxation process can take place around the S1S0-DHT intersection region. Once the ring-closure conformer returns to the ground state, the S0-DHT minimum will be generated with a large quantity of excess energy in its internal degrees of freedom, which will subsequently re-open to form the S0-OTP conformer. Besides, there are still a few trajectories (7.2%) survive in the S_1 state at the end of simulated period of 3.0 ps.

In addition, two relaxation time constants are obtained according to the di-exponential model. Specifically, the first time component is fitted to be 538.7 fs, which is in agreement with experimental value of 700.0 fs in solution of THF. The second time component is also well-reproduced by the present OM2-MRCI-based dynamical simulation (5.1 ps in this work *vs* 3.0 ps in TAS). The PRP experiment assigned the faster process to the nonreactive deactivation (PATH I) and the slower one to the ring-closure reaction (PATH II), which is also in line with our present calculations. Notably, the present work focuses on elucidating the fundamental gas-phase photochemical reaction pathways of OTP, and therefore solvent effects are not explicitly considered. However, solvent effects, such as mechanical and electrostatic interactions, can significantly influence the excited-state relaxation dynamics of OTP. Given their potential importance, these solvent effects will be systematically investigated in our future studies. Finally, the present work can provide important photocyclization mechanistic insights for OTP system and also the similar *ortho*-arenes.

Supporting Information

Active space, key structural parameters, structural overlaps, cartesian coordinates of stationary and intersection structures. Supporting information can be downloaded here.

Acknowledgments

This work was supported by the Open Project of State Key Laboratory of Synergistic Chem-Bio Synthesis (sklscbs202517), the Key Science and Technology Project of Jinhua City (2023-1-093), the Zhejiang Provincial Natural Science Foundation of China (No. LZ23B030001), the National Key Research and Development Program of China (No. 2019YFA0709400).

References

[1] Ward C.L., Elles C.G., Controlling the excited-state reaction dynamics of a photochromic molecular switch with sequential two-photon excitation. *J. Phys. Chem. Lett.,* **3** (2012), 2995–3000.

[2] Polli D., Altoe P., Weingart O., Spillane K.M., Manzoni C., Brida D., Tomasello G., Orlandi G., Kukura P., Mathies R.A., Garavelli M. and Cerullo G., Conical intersection dynamics of the primary photoisomerization event in vision. *Nature,* **467** (2010), 440–443.

[3] Lim J.S. and Kim S.K., Experimental probing of conical intersection dynamics in the photodissociation of thioanisole. *Nat. Chem.,* **2** (2010), 627–632.

[4] Levine B.G. and Martinez T.J., Isomerization through conical intersections. *Annu. Rev. Phys. Chem.,* **58** (2007), 613–634.

[5] Worth G.A. and Cederbaum L.S., Beyond Born–Oppenheimer molecular dynamics through a conical intersection. *Annu. Rev. Phys. Chem.,* **55** (2004), 127–158.

[6] Yarkony D.R., Conical intersections: the new conventional wisdom. *J. Phys. Chem. A,* **105** (2001), 6277–6293.

[7] Ehrler B., Wilson M.W.B., Rao A., Friend R.H. and Greenham N.C., Singlet exciton fission-sensitized infrared quantum dot solar cells. *Nano Lett.,* **12** (2012), 1053–1057.

[8] Rao A., Wilson M.W.B., Hodgkiss J.M., Albert-Seifried S., Bässler H. and Friend R.H., Exciton fission and charge generation via triplet excitons in pentacene/C60 bilayers. *J. Am. Chem. Soc.,* **132** (2010), 12698–12703.

[9] Zhu H.M., Yang Y., Wu K.F. and Lian T.Q., Charge transfer dynamics from photoexcited semiconductor quantum dots. *Annu. Rev. Phys. Chem.,* **67** (2016), 259–281.

[10] Laarhoven W.H., Cuppen T.J.H. and Nivard R.J.F., Photodehydrocyclizations in stilbene-like compounds. 2. photochemistry of distyrylbenzenes. *Tetrahedron,* **26** (1970), 1069–1083.

[11] Mallory F.B. and Mallory C.W., Organic reactions, volume 30. *John Wiley & Sons,* New York, 1984, 1–456.

[12] Wang Y.-T., Gao Y.-J., Wang Q. and Cui G.-L., Photochromic mechanism of a bridged diarylethene: combined electronic structure calculations and nonadiabatic dynamics simulations. *J. Phys. Chem. A,* **121** (2017), 793–802.

[13] Gao Y.-J., Chang X.-P., Liu X.-Y., Li Q.-S., Cui G.-L. and Thiel W., Excited-state decay paths in tetraphenylethene derivatives. *J. Phys. Chem. A,* **121** (2017), 2572–2579.

[14] Sato T., Shimada S. and Hata K., A new route to polycondensed aromatics: photolytic formation of triphenylene and dibenzo[fg,op]naphthacene ring systems. *Bull. Chem. Soc. Jpn.,* **44** (1971), 2484–2490.

[15] Kharasch N., Alston T.G., Lewis H.B. and Wolf W., Photochemical conversion of o-terphenyl into triphenylene. *Chem. Commun.,* **12** (1965), 242–243.

[16] Liu L.B., Yang B.W., Katz T.J. and Poindexter M.K., Improved methodology for photocyclization reactions. *J. Org. Chem.,* **56** (1991), 3769–3775.

[17] Wang J.-L., Zhao R., Dai J.-L., Jia P.-K., Yin B.-W., Wang H.-G. and Xie B.-B., A different photochromic mechanism of spirooxadiazine: electronic structure calculations and nonadiabatic dynamics simulations. *Dyes Pigm.,* **230** (2024), 112332.

[18] Wang K.-X., Yin B.-W., Jia P.-K., Zhang T.-S., Cui G.-L. and Xie B.-B., Electronic structure calculations and nonadiabatic dynamics simulations on reversible photochromic mechanism of spirooxazine. *Dyes Pigm.,* **205** (2022), 110509.

[19] Hou L.L., Zhang X.Y., Pijper T.C., Browne W.R. and Feringa B.L., Reversible photochemical control of singlet oxygen generation using diarylethene photochromic switches. *J. Am. Chem. Soc.,* **136** (2014), 910–913.

[20] Mallory F.B., Butler K.E., Berube A., Luzik E.D., Mallory C.W., Brondyke E.J., Hiremath R., Ngo P. and Carroll P.J., Phenacenes: a family of graphite ribbons. Part 3: iterative strategies for the synthesis of large phenacenes. *Tetrahedron,* **57** (2001), 3715–3724.

[21] Mallory F.B., Butler K.E., Evans A.C., Brondyke E.J., Mallory C.W., Yang C.Q. and Ellenstein A., Phenacenes: a family of graphite ribbons. 2. syntheses of some [7]phenacenes and an [11]phenacene by stilbene-like photocyclizations. *J. Am. Chem. Soc.,* **119** (1997), 2119–2124.

[22] Irie M., Diarylethenes for memories and switches. *Chem. Rev.,* **100** (2000), 1685–1716.

[23] Bach T. and Hehn J.P., Photochemical reactions as key steps in natural product synthesis. *Angew. Chem. Int. Ed.,* **50** (2011), 1000–1045.

[24] Singh S.B. and Pettit G.R., Antineoplastic agents. 166. isolation, structure, and synthesis of combretastatin C-1. *J. Org. Chem.,* **54** (1989), 4105–4114.

[25] Kelly T.R., Jagoe C.T. and Li Q., Synthesis of (±)-cervinomycin A1 and A2. *J. Am. Chem. Soc.,* **111** (1989), 4522–4524.

[26] Snyder J.A. and Bragg A.E., Ultrafast pump–repump–probe photochemical hole burning as a probe of excited-state reaction pathway branching. *J. Phys. Chem. Lett.,* **9** (2018), 5847–5854.

[27] Molloy M.S., Snyder J.A., DeFrancisco J.R. and Bragg A.E., Structural control of nonadiabatic photochemical bond formation: photocyclization in structurally modified ortho-terphenyls. *J. Phys. Chem. A,* **120** (2016), 3998–4007.

[28] Snyder J.A. and Bragg A.E., Structural control of nonadiabatic bond formation: the photochemical formation and stability of substituted 4a,4b-dihydrotriphenylenes. *J. Phys. Chem. A,* **119** (2015), 3972–3985.

[29] Molloy M.S., Snyder J.A. and Bragg A.E., Structural and solvent control of nonadiabatic photochemical bond formation: photocyclization of o-terphenyl in solution. *J. Phys. Chem. A,* **118** (2014), 3913–3925.

[30] Smith M.C., Snyder J.A., Streifel B.C. and Bragg A.E., Ultrafast excited-state dynamics of ortho-terphenyl and 1,2-diphenylcyclohexene: the role of ethylenic twisting in the nonadiabatic photocyclization of stilbene analogs. *J. Phys. Chem. Lett.,* **4** (2013), 1895–1900.

[31] Ishii K., Takeuchi S. and Tahara T., A 40-fs time-resolved absorption study on cis-stilbene in solution: observation of wavepacket motion on the reactive excited state. *Chem. Phys. Lett.,* **398** (2004), 400–406.

[32] Quenneville J. and Martinez T.J., Ab initio study of cis–trans photoisomerization in stilbene and ethylene. *J. Phys. Chem. A,* **107** (2003), 829–837.

[33] Rodier J.M. and Myers A.B., Cis-stilbene photochemistry: solvent dependence of the initial dynamics and quantum yields. *J. Am. Chem. Soc.,* **115** (1993), 10791–10795.

[34] Waldeck D.H., Photoisomerization dynamics of stilbenes. *Chem. Rev.,* **91** (1991), 415–436.

[35] Frederick J.H., Fujiwara Y., Penn J.H., Yoshihara K. and Petek H., Models for stilbene photoisomerization: experimental and theoretical studies of the excited-state dynamics of 1,2-diphenylcycloalkenes. *J. Phys. Chem.,* **95** (1991), 2845–2858.

[36] Petek H., Yoshihara K., Fujiwara Y., Zhe L., Penn J.H. and Frederick J.H., Is the nonradiative decay of S1 cis-stilbene due to the dihydrophenanthrene isomerization channel? suggestive evidence from photophysical measurements on 1,2-diphenylcycloalkenes. *J. Phys. Chem.,* **94** (1990), 7539–7543.

[37] Muszkat K.A. and Fischer E., Structure, spectra, photochemistry, and thermal reactions of the 4a,4b-dihydrophenanthrenes. *J. Chem. Soc. B: Phys. Org.,* **1967** (1967), 662–678.

[38] Gegiou D., Muszkat K.A. and Fischer E., Temperature dependence of photoisomerization. VI. the viscosity effect. *J. Am. Chem. Soc.,* **90** (1967), 12–18.

[39] Vosko S.H., Wilk L. and Nusair M., Accurate spin-dependent electron liquid correlation energies for local spin density calculations: a critical analysis. *Can. J. Phys.,* **58** (1980), 1200–1211.

[40] Becke A.D., Density-functional exchange-energy approximation with correct asymptotic behavior. *Phys. Rev. A,* **38** (1988), 3098–3100.

[41] Lee C.T., Yang W.T. and Parr R.G., Development of the Colle–Salvetti correlation-energy formula into a functional of the electron density. *Phys. Rev. B,* **37** (1988), 785–789.

[42] Becke A.D., A new mixing of Hartree–Fock and local density-functional theories. *J. Chem. Phys.,* **98** (1993), 1372–1377.

[43] Parr R.G. and Yang W.T., *Density-Functional Theory of Atoms and Molecules,* Oxford University Press, Oxford, 1994.

[44] Yanai T., Tew D.P. and Handy N.C., A new hybrid exchange-correlation functional using the Coulomb-attenuating method (CAM-B3LYP). *Chem. Phys. Lett.,* **393** (2004), 51–57.

[45] Marques M.A.L., Ullrich C.A., Nogueira F., Rubio A., Burke K. and Gross E.K.U., *Time-Dependent Density Functional Theory,* Springer, Berlin, 2006.

[46] Andersson K., Malmqvist P.A., Roos B.O., Sadlej A.J. and Wolinski K., Second-order perturbation theory with a CASSCF reference function. *J. Phys. Chem.,* **94** (1990), 5483–5488.

[47] Andersson K., Malmqvist P.A. and Roos B.O., Second-order perturbation theory with a complete active space self-consistent field reference function. *J. Chem. Phys.,* **96** (1992), 1218–1226.

[48] Ghigo G., Roos B.O. and Malmqvist P.A., A modified definition of the zeroth-order Hamiltonian in multiconfigurational perturbation theory (CASPT2). *Chem. Phys. Lett.,* **396** (2004), 142–149.

[49] Forsberg N. and Malmqvist P.A., Multiconfiguration perturbation theory with imaginary level shift. *Chem. Phys. Lett.,* **274** (1997), 196–204.

[50] Aquilante F., Lindh R. and Pedersen T.B., Unbiased auxiliary basis sets for accurate two-electron integral approximations. *J. Chem. Phys.,* **127** (2007), 114107.

[51] Ditchfield R., Hehre W.J. and Pople J.A., Self-consistent molecular orbital methods. extended Gaussian-type basis for molecular-orbital studies of organic molecules. *J. Chem. Phys.,* **54** (1971), 724–728.

[52] Francl M.M., Pietro W.J., Hehre W.J., Binkley J.S., Gordon M.S., DeFrees D.J. and Pople J.A., Self-consistent molecular orbital methods. XXIII. a polarization-type basis set for second-row elements. *J. Chem. Phys.,* **77** (1982), 3654–3665.

[53] Frisch M.J., Trucks G.W., Schlegel H.B., et al., Gaussian 09, revision A.02. *Gaussian, Inc.,* Wallingford CT, 2009.

[54] Karlström G., Lindh R., Malmqvist P.A., et al., MOLCAS: a program package for computational chemistry. *Comput. Mater. Sci.,* **28** (2003), 222–239.

[55] Aquilante F., De Vico L., Ferré N., et al., Software news and update MOLCAS 7: the next generation. *J. Comput. Chem.,* **31** (2010), 224–247.

[56] Yarkony D.R., Nuclear dynamics near conical intersections in the adiabatic representation: I. the effects of local topography on interstate transitions. *J. Chem. Phys.,* **114** (2001), 2601–2613.

[57] Keal T.W., Koslowski A. and Thiel W., Comparison of algorithms for conical intersection optimisation using semiempirical methods. *Theor. Chem. Acc.,* **118** (2007), 837–844.

[58] Granucci G., Persico M. and Zoccante A., Including quantum decoherence in surface hopping. *J. Chem. Phys.,* **133** (2010), 134111.

[59] Weber W. and Thiel W., Orthogonalization corrections for semiempirical methods. *Theor. Chem. Acc.,* **103** (2000), 495–506.

[60] Koslowski A., Beck M.E. and Thiel W., Implementation of a general multireference configuration interaction procedure with analytic gradients in a semiempirical context using the graphical unitary group approach. *J. Comput. Chem.,* **24** (2003), 714–726.

[61] Thiel W., MNDO99 program, version 6.1. *Max-Planck-Institut für Kohlenforschung,* Mülheim, 2007.

[62] Xie B.-B., Xia S.-H., Liu L.-H. and Cui G.-L., Surface-hopping dynamics simulations of malachite green: a

triphenylmethane dye. *J. Phys. Chem. A,* **119** (2015), 5607–5617.

[63] Liu X.-Y., Chang X.-P., Xia S.-H., Cui G.-L. and Thiel W., Excited-state proton-transfer-induced trapping enhances the fluorescence emission of a locked GFP chromophore. *J. Chem. Theory Comput.,* **12** (2016), 753–764.

[64] Wang Y.-T., Liu X.-Y., Cui G.-L., Fang W.-H. and Thiel W., Photoisomerization of arylazopyrazole photoswitches: stereospecific excited-state relaxation. *Angew. Chem. Int. Ed.,* **55** (2016), 14009–14013.

[65] Xie B.-B., Xia S.-H., Chang X.-P. and Cui G.-L., Photophysics of Auramine-O: electronic structure calculations and nonadiabatic dynamics simulations. *Phys. Chem. Chem. Phys.,* **18** (2016), 403–413.

[66] Götze J.P., Anders F., Petry S., Witte J.F. and Lokstein H., Spectral characterization of the main pigments in the plant photosynthetic apparatus by theory and experiment. *Chem. Phys.,* **559** (2022), 111517.

[67] Viel A., Krawczyk R.P., Manthe U. and Domcke W., The sudden-polarization effect and its role in the ultrafast photochemistry of ethene. *Angew. Chem. Int. Ed.,* **42** (2003), 3434–3436.